J. Fluid Mech. (2014), *vol.* 745, *pp.* 164–179. © Cambridge University Press 2014
doi:10.1017/jfm.2014.85

Crossover between two- and three-dimensional turbulence in spatial mixing layers

Luca Biancofiore†

Laboratoire J. A. Dieudonné, Université de Nice – Sophia Antipolis, Parc Valrose, F-06108 Nice CEDEX 02, France

Linné Flow Centre, KTH Mechanics, SE-100 44 Stockholm, Sweden

Department of Mechanical Engineering, Imperial College London, Exhibition Road, South Kensington, London SW7 2AZ, UK

(Received 24 April 2013; revised 7 January 2014; accepted 7 February 2014; first published online 18 March 2014)

We investigate how the domain depth affects the turbulent behaviour in spatially developing mixing layers by means of large-eddy simulations based on a spectral vanishing viscosity technique. Analyses of spectra of the vertical velocity, of Lumley's diagrams, of the turbulent kinetic energy and of the vortex stretching show that a two-dimensional behaviour of the turbulence is promoted in spatial mixing layers by constricting the fluid motion in one direction. This finding is in agreement with previous works on turbulent systems constrained by a geometric anisotropy, pioneered by Smith, Chasnov & Waleffe (*Phys. Rev. Lett.*, vol. 77, 1996, pp. 2467–2470). We observe that the growth of the momentum thickness along the streamwise direction is damped in a confined domain. An almost fully two-dimensional turbulent behaviour is observed when the momentum thickness is of the same order of magnitude as the confining scale.

Key words: shear layer turbulence, shear layers, turbulent flows

1. Introduction

A comprehensive understanding of two-dimensional (2D) turbulence is crucial to many domains. For instance, large-scale motions in the atmosphere or oceans are described, to first approximation, as 2D turbulent fluids. Although most physical fluid systems are intrinsically three-dimensional (3D), the motion can be constrained in one spatial direction, which leads to approximately 2D fluid motions. Several methods have been applied in order to implement such a constraint. In particular, there are two main types of constraint: (i) body forces, including buoyancy, rotation and magnetic fields; and (ii) geometric anisotropy, which forces the length scale in one direction to be much smaller than the length scales in the other two. In geophysical and astrophysical systems, both kinds of constraints may be relevant. Boffetta & Ecke (2012) have extensively illustrated the first constraint in their review. In this paper, we focus on the second type.

Analyses of the two-dimensionalization due to geometric anisotropy can be useful to treat some aspects of motion in the atmosphere or oceans, since the depth of

† Email address for correspondence: lbiancof@imperial.ac.uk

https://doi.org/10.1017/jfm.2014.85 Published online by Cambridge University Press

the atmosphere (or ocean) is much smaller, ~ 10 km, than the lateral global scales, 10^3–10^4 km. In particular, these geophysical flows are often represented by balanced models, which effectively filter out the unbalanced or 3D modes. Therefore, the study of the feedback of the unbalanced modes on the 2D base flow is crucial (Ngan, Straub & Bartello 2008). In particular, the effect of a geometric anisotropy on such feedback and on the 3D perturbation can have implications in the atmosphere and ocean (Ngan, Straub & Bartello 2005). The flows analysed in the present paper obviously represent an idealization, since stratification, rotation and forcing are neglected. However, they can be useful as prototypes for more realistic ones.

Smith, Chasnov & Waleffe (1996) were the first to study the effects of aspect ratio on turbulent motions. They analysed forced rotating turbulent flows in a domain with small aspect ratio. In particular, they noticed that small-scale 3D turbulence, characterized by a forward cascade of kinetic energy, can coexist with a 2D inverse cascade, which takes place at scales larger than the scale of the confinement. A similar result was also obtained by Celani, Musacchio & Vincenzi (2010). A number of studies have been conducted on this subject, starting from the pioneering study of Smith *et al.* (1996). Several kinds of flows have been examined, such as freely decaying turbulence (Ngan *et al.* 2005), electromagnetically driven flows (Shats, Byrne & Xia 2010; Xia *et al.* 2011) and Rayleigh–Taylor convection (Boffetta *et al.* 2012). All these studies have shown that confinement induces a reduction of dimensionality of the system, especially at large scales, from 3D to 2D behaviour.

Shear instabilities appear in several kinds of flows, such as wakes, jets or mixing layers. Such flows are encountered in aerodynamics, in the atmosphere or the ocean (e.g. in the wake of mountains, in the Gulf Stream, etc.) as well as in the atmospheres of Jupiter or Saturn (at the interface between neighbouring zonal jets). In particular, the mixing layer between two flows of velocities U_1 and U_2 can be viewed as the prototype flow of free shear flows. Brown & Roshko (1974) found that large-scale coherent structures are intrinsic features of turbulent mixing layers. Furthermore, Winant & Browand (1974) described how the sequential mergings of vortices provide the primary mechanisms for the spreading of the layer along the downstream direction. An extensive review of this subject has been given by Ho & Huerre (1984). The important parameters that characterize a mixing layer are: (i) the velocity ratio $R = \Delta U/(2U_a)$, which measures the magnitude of the total shear $\Delta U = U_1 - U_2$ compared with the average velocity $U_a = (U_1 + U_2)/2$; (ii) the initial (or at the entry) momentum thickness, $\theta_e = \int_{-\infty}^{+\infty} \left[0.25 - \left(\frac{U_e(y)-U_a}{\Delta U}\right)^2\right] \mathrm{d}y$ (where $U_e(y)$ is the velocity profile of the mixing layer), which is a measure of the thickness between the two streams; and (iii) the Reynolds number, $Re = \Delta U \theta_e/\nu$, where ν is the kinematic viscosity. One example of a mixing layer profile is given in figure 1.

The three-dimensionalization of a canonical plane mixing layer has also been investigated. The main rolls due to the primary 2D instability can be deformed by coherent spanwise structures created by a secondary instability mechanisms. Two different secondary instabilities were found (Pierrehumbert & Widnall 1982): (i) a pair of conjugate subharmonic modes yielding helical pairings (Chandrsuda *et al.* 1978); and (ii) a streamwise-independent mode making the primary vortices oscillate in phase in the spanwise direction (Bernal & Roshko 1986). Comte and coworkers (Comte, Lesieur & Lamballais 1992; Comte, Silvestrini & Bégou 1998) have noticed that wide domains favour the highly 3D helical pairings. In particular, the primary and secondary vortices strongly interact with each other, reinforcing the vorticity magnitude (Comte *et al.* 1998).

https://doi.org/10.1017/jfm.2014.85 Published online by Cambridge University Press

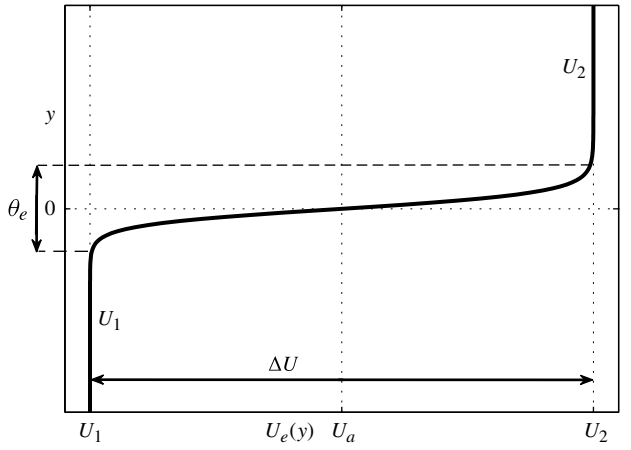


FIGURE 1. An example of the velocity profile of a mixing layer.

Despite the importance of turbulent shear flows, no significant efforts have been made to study the influence of geometric anisotropy on such flows. Recently, Biancofiore, Gallaire & Pasquetti (2012) made some preliminary studies of aspect ratio effects on spatial developing turbulent wakes. They found that a decrease of the ratio between the depth and height of the domain damped the 3D motion of the turbulence. Their main goal was to study the effect of the blockage along the wall-normal direction on the turbulence strength rather than analyse the aspect ratio effects.

The main aim of the present work is to study the aspect ratio effects in a spatial developing shear flow. To do this, we introduce a geometric anisotropy in a spatial turbulent mixing layer (i.e. the prototype of a shear flow) by constraining the motion along the spanwise direction. Large-eddy simulations based on a spectral vanishing viscosity (SVV-LES) approach are conducted with the aim to unveil how a reduction in the depth of the domain influences the turbulent behaviour. The numerical method has already been used in different physical fluid systems, such as Ahmed's body flow (Minguez, Pasquetti & Serre 2008), thermal stratified wakes (Pasquetti 2010) or obstacle-free wakes (Biancofiore *et al.* 2012). While the LES approach cannot properly describe the smallest structures, it is still valid in order to simulate specific aspects of shear-dominated flows (see e.g. Picano & Hanjalić 2012). The outline of the paper is as follows: § 2 describes the model and the numerical method; in § 3 an analysis of the effect of variations in the depths of turbulent mixing layers is carried out; finally, conclusions are drawn in § 4.

2. Model and numerical method

In this section, we describe the numerical method used in our simulations. The model is described in § 2.1 along with the conditions at the boundaries. In § 2.2 we briefly describe both the spatial approximation and the time scheme. Afterwards, the spectral vanishing viscosity technique is illustrated in § 2.3. Finally, in § 2.4 we describe the numerical details of our computations. Additional information on the numerical method may be found in, for example, Pasquetti (2006), Minguez *et al.* (2008) and the references therein.

https://doi.org/10.1017/jfm.2014.85 Published online by Cambridge University Press

2.1. *Model and boundary conditions*

The flow is assumed to be governed by the incompressible dimensionless Navier–Stokes equations

$$\partial_t \boldsymbol{u} + \boldsymbol{u}\cdot\boldsymbol{\nabla}\boldsymbol{u} = -\boldsymbol{\nabla}p + Re^{-1}\Delta\boldsymbol{u} \quad \text{in } \Omega\times(0,t_f), \tag{2.1}$$

$$\boldsymbol{\nabla}\cdot\boldsymbol{u} = 0, \tag{2.2}$$

$$B(\boldsymbol{u}) = \boldsymbol{g} \quad \text{on } \Gamma\times(0,t_f), \tag{2.3}$$

$$\boldsymbol{u}|_{t=0} = \boldsymbol{u}_0 \quad \text{in } \Omega, \tag{2.4}$$

where t (respectively t_f) is the time (final time), Ω is the computational domain and Γ its boundary, $\boldsymbol{u} = (u, v, w)$ is the velocity, p is the pressure and Re is the Reynolds number. The boundary operator B and the function $\boldsymbol{g}$ are used to express the boundary conditions. The geometry is channel-like in the x (streamwise/horizontal) and y (crossflow/vertical) directions, while the z (spanwise) direction is periodic.

At the inlet, we impose the velocity profile of a mixing layer (see figure 1) plus a random perturbation of amplitude 10^{-3}, i.e. $\boldsymbol{u}_e = (U_e(y), 0, 0)$. The difference in the velocities is settled to $\Delta U = 1$, while the average velocity is $U_a = 1$. The momentum thickness of the profile is $\theta_e = 0.0141$. For the definition of these parameters, see § 1. The velocity and length reference scales are $V = \Delta U$ and $L = \theta_e/0.0141$, respectively. Therefore, the Reynolds number based on V and L is $Re = 66\,667$. However, it is $Re_\theta = (\Delta U\,\theta_e)/\nu = 94$ if based on the common mixing layer reference scales, i.e. the difference in the velocities ΔU and the momentum thickness θ_e. At the sidewalls, free slip conditions are applied.

At the end of the domain, we use a convective condition based on the flow-rate velocity U_f. With n for the time advancement index, at the outlet $x = x_{out}$ we thus enforce

$$\boldsymbol{u}(x_{out}, t_{n+1}) = \boldsymbol{u}(x_{out} - U_f(t_{n+1} - t_n), t_n). \tag{2.5}$$

The use of a Lagrangian rather than an Eulerian formulation allows one to localize best the influence of the outflow boundary conditions. Moreover, the streamwise outlet profile is slightly adjusted to be consistent with the divergence-free constraint, i.e. so that the outlet flow rate exactly equals the inlet one.

2.2. *Spatial approximation and time scheme*

The numerical method is based on a multi-domain Chebyshev–Fourier approximation. In the streamwise direction, we use a domain decomposition technique. The code is vectorized and parallelized (one subdomain per processor). In each subdomain, the continuity of the solution at the subdomain interfaces is ensured by using an extended influence matrix technique (Sabbah & Pasquetti 1998). In each subdomain, the spatial approximation is based on a collocation Chebyshev method in the crossflow and streamwise directions, whereas a Fourier–Galerkin method is used along the periodic spanwise direction. Moreover, we use a suitable mapping along the crossflow direction in order to accumulate grid points where the two streams mix, i.e. around the centreline $y = 0$.

The time scheme is based on a fractional step method and is globally second-order accurate. Three steps are involved:

(i) An explicit transport step based on an 'operator integration factor' semi-Lagrangian method and a fourth-order Runge–Kutta scheme is used to handle the nonlinear convective terms.

https://doi.org/10.1017/jfm.2014.85 Published online by Cambridge University Press

(ii) An implicit diffusion step is used to handle the linear viscous term. Time derivatives of the velocity components are approximated at the resolution time t_{n+1}, while the pressure is expressed at time t_n following the so-called Goda scheme, to obtain a provisional velocity.

(iii) A projection step is used to obtain a divergence-free velocity field. It is based on a unique grid 'P_N–P_{N-2}' approximation, i.e. the polynomial degree for the pressure is two degrees less than that for the velocity components. In this way, no boundary conditions are required for the pressure, and in addition the discrete problem is well posed (no 'pressure spurious modes'). In our case, such P_N–P_{N-2} approximation has been extended to a multi-domain approximation. Then, unknown values of the pressure are only defined in the inner grid points, including the subdomain interface points.

2.3. *Spectral vanishing viscosity approach*

In this section, we describe the numerical approach to implement the large-eddy simulation (LES) capability: the spectral vanishing viscosity (SVV) technique (Maday, Ould Kaber & Tadmor 1993). This technique consists of introducing artificial viscosity in the high-frequency range of the spectral approximation. The definition of the SVV stabilization term V_N is given according to Maday *et al.* (1993), who have resolved in the interval $(-1, 1)$ the inviscid 1D Burgers equation by means of the spectral Legendre method. In this case, with N for the degree of the polynomial approximation, we have

$$V_N = \epsilon_N \partial_x Q_N(\partial_x u_N), \tag{2.6}$$

where u_N is the numerical approximation of some exact solution u, ϵ_N is the amplitude coefficient (of the order of $O(N^{-1})$) and Q_N is the 'SVV operator'. The Legendre polynomial of degree k, L_k, is defined from

$$Q_N\phi = \sum_{k=0}^{N} \hat{Q}_k \hat{\phi}_k L_k, \quad \forall\ \phi \text{ such that } \phi = \sum_{k=0}^{N} \hat{\phi}_k L_k, \tag{2.7}$$

where $\hat{Q}_k = 0$ if $k \leqslant m_N$ and $0 < \hat{Q}_k \leqslant 1$ if $k > m_N$. As suggested in Maday *et al.* (1993), we use a smooth variation for the coefficients $\hat{Q}_k$:

$$\hat{Q}_k = \exp\left[-\left(\frac{N-k}{m_N-k}\right)^2\right] \quad \text{for } k > m_N. \tag{2.8}$$

The values of the amplitude coefficient ϵ_N and the threshold frequency m_N must be a compromise between the accuracy of the SVV solution and the stability of the numerical scheme. In the wake of a cylinder, Pasquetti (2005) has found that the best results were obtained for the largest value of m_N and the smallest value of ϵ_N. Therefore, the following choice has been made: (i) $m_N = \sqrt{N}$, whereas $m_N = N/2$, which is, for example, used in Karamanos & Karniadakis (2000), was not found to be stabilizing enough; and (ii) $\epsilon_N = 1/N$. The corresponding spectral kernel $\hat{Q}_k$ of the SVV operators is shown in figure 2(*a*) for the values of N used in this paper (see § 2.4). In our multi-dimensional framework, such an SVV term may be extended to

$$Su_i = \epsilon_N \nabla \cdot Q(\nabla u_i), \tag{2.9}$$

with u_i any component of $\boldsymbol{u}$ and where Q applies independently to each component of ∇u_i. The reader is referred to Xu & Pasquetti (2004) for more details on such

https://doi.org/10.1017/jfm.2014.85 Published online by Cambridge University Press

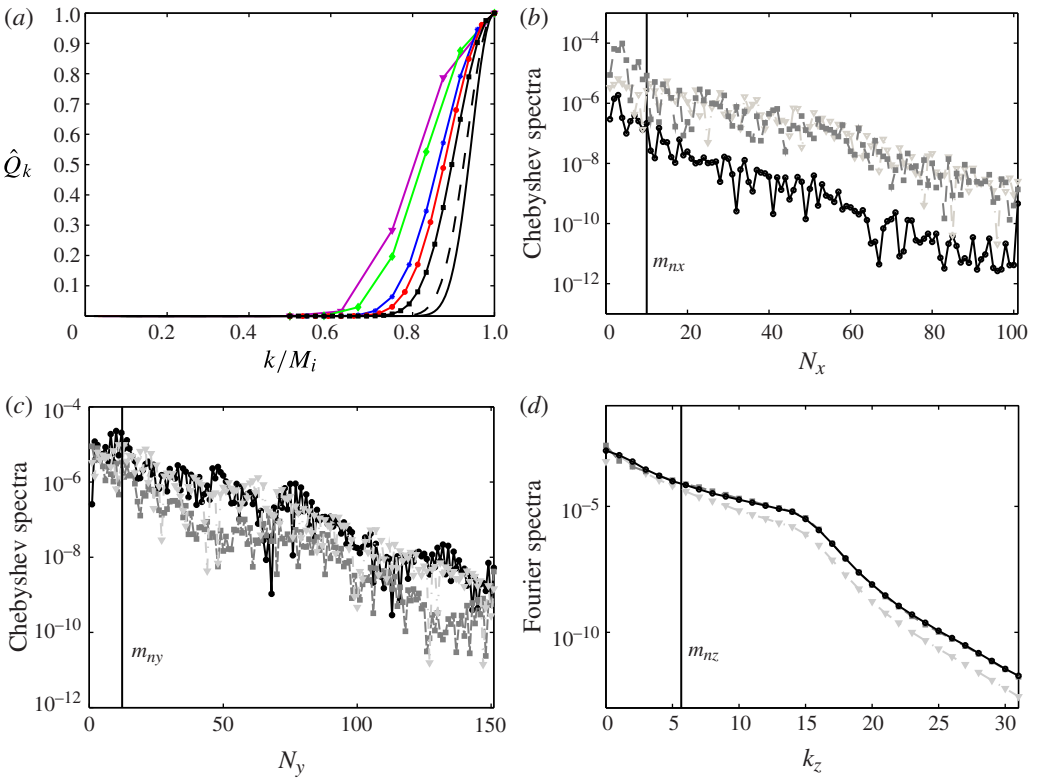


FIGURE 2. (Colour online) (*a*) Spectral kernel of the one-dimensional SVV operator for different values of the threshold frequency m_N. The continuous line without symbols depicts $N = 150$, the dashed line $N = 100$, and lines with squares $N = 48$, circles $N = 32$, asterisks $N = 24$, diamonds $N = 12$ and triangles $N = 8$. (*b–d*) Spectra of the velocity fluctuations: (*b*) x Chebyshev, (*c*) y Chebyshev, (*d*) z Fourier. The black lines depict the u component, the dark grey the v component and the light grey the w component.

an extension of the initial 1D definition. The threshold frequency and the amplitude coefficient are chosen equal for the three directions. A typical phenomenon in transitional turbulent shear flows, such as the spatial mixing layers analysed in this study, is the backscattering, i.e. the local transfer of energy from the small to the large scales. Such a phenomenon is inaccessible in standard LES, such as the Smagorinsky model, while our SVV-LES model allows the transfer from small to large scales, as explained by Biancofiore *et al.* (2012). However, this modelled backscattering could be more numerical than physical; see Cholet & Lesieur (1981) for a more physical approach.

2.4. *Numerical details and resolution*

In the present paper, we call length L_x, height L_y and depth L_z the sizes of the domain along the x, y and z directions, respectively. The computational domain is $(0, L_x) \times (-L_y/2, L_y/2) \times (-L_z/2, L_z/2)$, where L_x and L_y were set to $L_x = 24$ and $L_y = 6$, respectively, while L_z has been varied over $0.125 \leqslant L_z \leqslant 6$. Note that the length unit is $L = \theta_e/0.0141$. We have generally used six subdomains, and in each of them the polynomial approximation degree in the x and y directions are set to $N_x = 100$ and

https://doi.org/10.1017/jfm.2014.85 Published online by Cambridge University Press

$N_y = 150$, respectively. Depending on L_z, we have varied the polynomial approximation degree in the z direction between $8 \leqslant N_z \leqslant 48$, which corresponds to a number of grid points M_z in the range $16 \leqslant M_z \leqslant 96$.

As initial condition, we have imposed the inlet conditions (see § 2.1) in all the domain. The computations have been carried out until a final time $t_f = 160$, where the time unit is equal to $T = L/V = \theta_e/(0.0141\Delta U)$. The dimensionless time step was set to $\Delta t = 2.5 \times 10^{-3}$. Finally, we have compared the statistics of the Reynolds stresses (i.e. a second-order momentum) over the last 50, 75 and 100 time units (for 60, 85, $110 \leqslant t \leqslant 160$, respectively) after the evacuation of the residuals of the initial condition. The maximal difference between the Reynolds stress averaged over 75 and 100 time units was found to be of the order of 10^{-5}. Then, we have concluded that the statistics have been converged over $60 \leqslant t \leqslant 160$.

The numerical resolution has been checked by analysing Fourier and Chebyshev 1D spectra of the velocity component fluctuations (u', v', w') averaged in time for the case with $L_z = 2$ (and $N_f = 32$); see figure 2(*b–d*). In particular, in figure 2(*b*) the x Chebyshev spectra have been computed in the last four subdomains and averaged along both the wall-normal and the spanwise directions; in figure 2(*c*) the y Chebyshev spectra have been averaged for $x \geqslant 8$ (i.e. the last four subdomains) and along the spanwise direction; and in figure 2(*d*) the Fourier spectra have been averaged for $x \geqslant 8$ and along the wall-normal direction. Spectral decays of more than two orders of magnitude indicate a satisfactory numerical result. We notice that all the spectra show that the dissipation is essentially active from the threshold frequency m_N (indicated in the figures) of the SVV stabilization. Note that satisfactory spectral decays only indicate an adequate resolution of the equations that are solved numerically, i.e. the SVV stabilized the Navier–Stokes equations, but of course do not provide a validation of this modelling. The spectra for the other values of the depth L_z examined in this study show similar tendencies. It should be noted that the SVV dissipation acts in the physical space on different scale lengths if we vary the domain size with the same resolution. However, tests with using different resolutions but keeping constant the value of the depth have given negligible variations in the spatial spectra and in the main results of this paper.

3. From three- to two-dimensional turbulence

Figure 3 shows the instantaneous modulus of the vorticity ω in the planes (*a–c*) x–y at $z = 0$ and (*d–f*) x–z at $y = 0$, at the final time $t_f = 160$ for different values of the depth of the domain: (*a*,*d*) $L_z = 2$, (*b*,*e*) $L_z = 1$ and (*c*,*f*) $L_z = 0.25$. For $L_z = 2$, the mixing layer is characterized by a completely 3D turbulent behaviour. If we decrease the depth to $L_z = 1$, large-scale 2D turbulent structures can be noticed. However, 3D structures are also present at small scales, so this configuration seems to have a halfway 2D–3D turbulent nature. Examples of this kind of turbulent behaviour were found, for instance, by Smith *et al.* (1996) or, in thermal convection, by Boffetta *et al.* (2012). Finally, for $L_z = 0.25$, the mixing layer seems to be completely characterized by 2D turbulent structures. Thus, a two-dimensionalization of the turbulence in a spatial mixing layer is created by a confinement in the spanwise direction. Similar results were obtained in forced turbulent systems (Celani *et al.* 2010), freely decaying turbulence (Ngan *et al.* 2005), electromagnetically driven flows (Shats *et al.* 2010; Xia *et al.* 2011) and Rayleigh–Taylor convection (Boffetta *et al.* 2012).

Furthermore, figure 3(*c*) illustrates typical mergings of vortices, which is indeed the primary process governing the streamwise growth of the mixing layer, as demonstrated

https://doi.org/10.1017/jfm.2014.85 Published online by Cambridge University Press

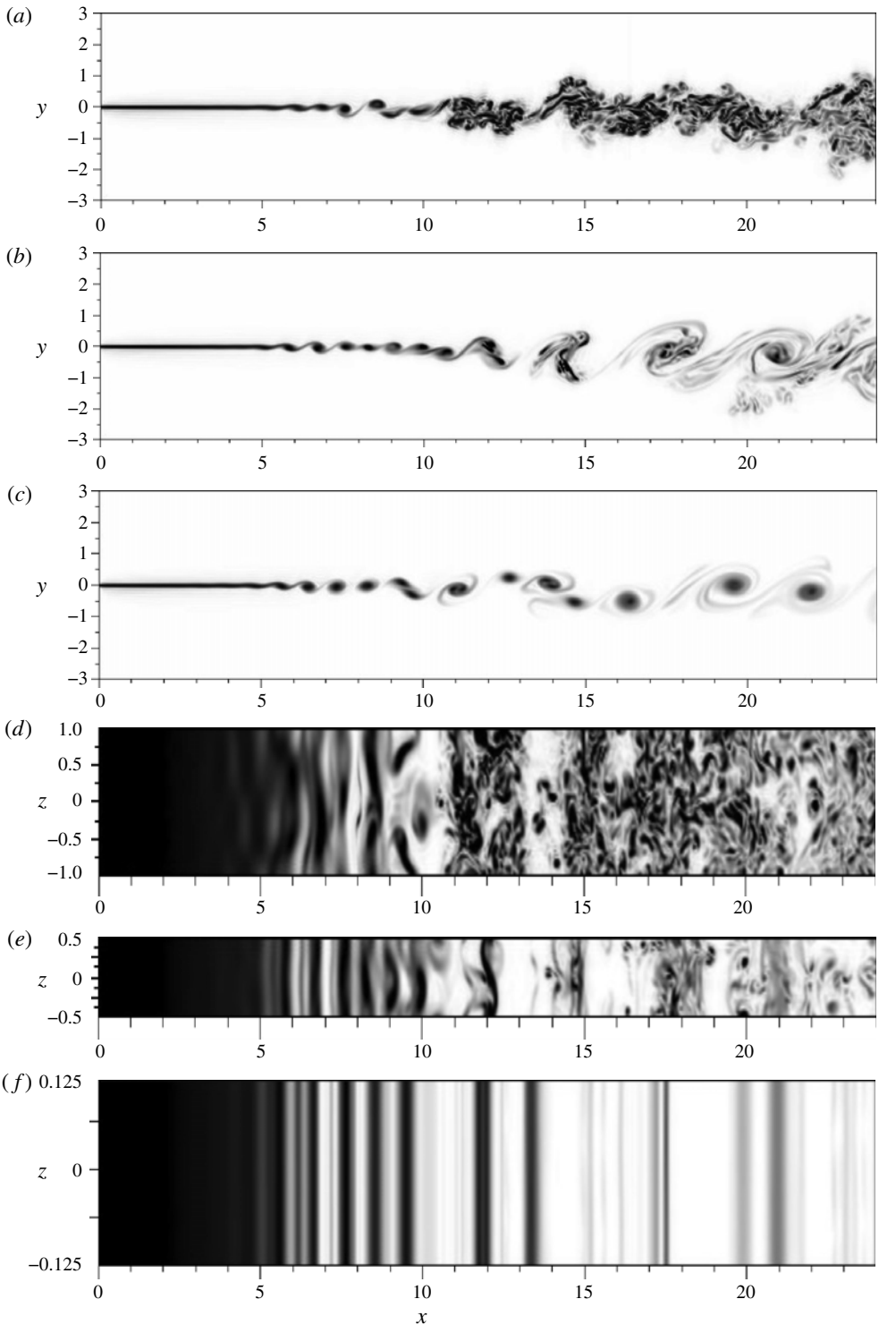


FIGURE 3. Instantaneous modulus of the vorticity $|\boldsymbol{\omega}|$ in the planes (*a–c*) x–y at $z = 0$ and (*d–f*) x–z at $y = 0$, at $t_f = 160$ for (*a,d*) $L_z = 2$, (*b,e*) $L_z = 1$ and (*c,f*) $L_z = 0.25$. Note that panel (*f*) is enlarged with respect to the real sizes.

https://doi.org/10.1017/jfm.2014.85 Published online by Cambridge University Press

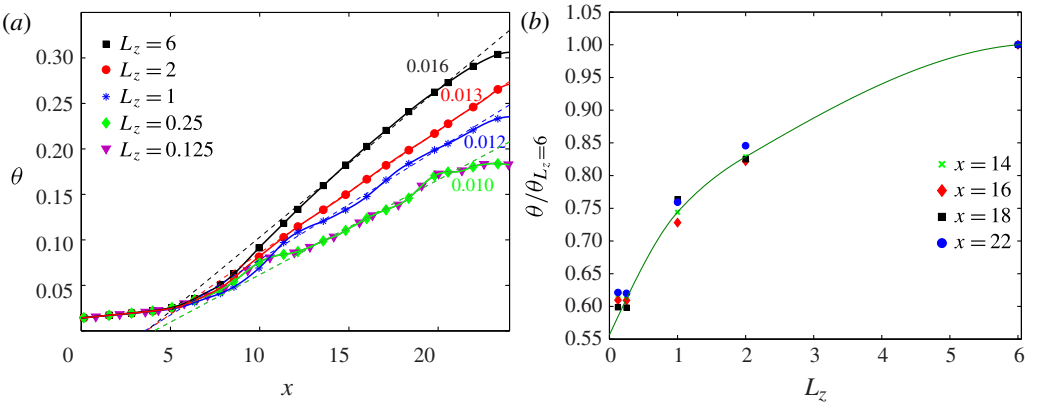


FIGURE 4. (Colour online) (*a*) Growth of the momentum thickness θ along the streamwise direction x. The dashed lines represent a linear approximation of the growth of the momentum thickness. (*b*) Momentum thickness versus L_z in different positions along the streamwise direction.

by Winant & Browand (1974). A comprehensive description of this vortex-merging scenario can be found in Ho & Huerre (1984).

3.1. *Growth of the momentum thickness*

In each streamwise location x along the domain, we compute the value of the momentum thickness, $\theta(x) = \int_{-L_y/2}^{+L_y/2} \left[0.25 - \left(\frac{\tilde{u}(x,y)-U_a}{\Delta U}\right)^2\right] \mathrm{d}y$, where the bar indicates averaging in time and over the z direction. Figure 4(*a*) illustrates the growth of the momentum thickness for different depths L_z. This growth is linear for each L_z. An approximately constant spreading rate $\mathrm{d}\theta/\mathrm{d}x$ is a well-known result (Ho & Huerre 1984). However, the spreading rate depends on the depth, as shown in figure 4(*a*). In particular, it decreases by increasing the confinement in the z direction. One can also note that the smallest domains $L_z = 0.25$ and $L_z = 0.125$ (depicted by diamonds and triangles, respectively) have an equal behaviour of the spreading rate. The largest domain $L_z = 6$ (depicted by squares) has a slope of 0.016, while the slopes for the smallest ones ($L_z = 0.25$ and $L_z = 0.125$) is 0.010. A value of 0.011 was experimentally found by Winant & Browand (1974) in a 2D turbulent spatial mixing layer.

Furthermore, the momentum thickness variation with the depth at given x locations of the domain is shown in figure 4(*b*). We have rescaled the momentum thickness using its value for $L_z = 6$. With the exclusion of the case with $L_z = 0.125$, we notice that the momentum thickness increases on enlarging the domain. The evolution seems to be not linear, but equal in each x location.

3.2. *Two-dimensionalization*

The analysis of the momentum thickness growth has shown that a variation in the depth of the domain can significantly modify the spreading of the mixing layer itself. However, it does not show whether a constraint in the spanwise direction means also a two-dimensionalization of the turbulent field. To study this aspect, we use Taylor's hypothesis to trace the temporal spectra (figure 5*a*) of the vertical velocity averaged for some values of z at $x = 14$ and $y = 0$ for $L_z = 2$, $L_z = 1$ and $L_z = 0.25$,

https://doi.org/10.1017/jfm.2014.85 Published online by Cambridge University Press

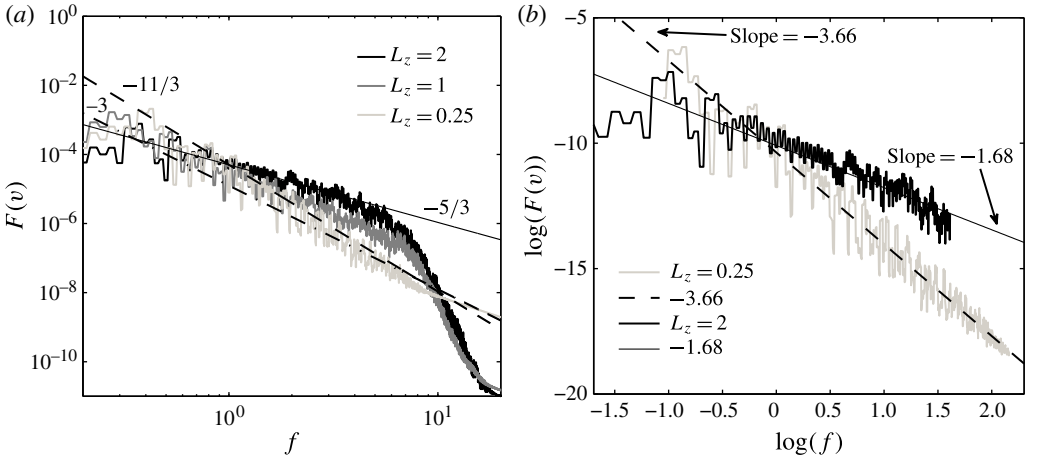


FIGURE 5. (*a*) Temporal spectra of the vertical velocity v at $x = 14$, $y = 0$ and averaged for some values of z. The bold black lines depict the spectra for $L_z = 2$, dark grey for $L_z = 1$ and light grey for $L_z = 0.25$. The thin lines represent possible theoretical values of the slope of the spectra: $-5/3$ (continuous line), $-11/3$ (dashed line) and -3 (dash-dotted line). (*b*) Power-law fit of the logarithmic values of the temporal spectra shown in panel (*a*). The legend is the same as for (*a*). The slope of the spectra in the inertial subrange for $L_z = 2$ and $L_z = 0.25$ is $-5/3$ and $-11/3$, respectively.

depicted by bold black, dark grey and light grey lines, respectively. The spectrum for $L_z = 2$ has a slope of $-5/3$ (depicted by thin continuous black line) in the inertial subrange. This is a sign of the presence of a direct energy cascade, which is a typical behaviour of 3D turbulent flows. If we decrease the depth to $L_z = 1$, we notice that the slope differs from $-5/3$. In particular, the magnitude of the spectral exponent of the spectrum increases. For $L_z = 0.25$, we expect that this magnitude continues to decrease until the value of -3. Theoretically, such a value means the presence of an enstrophy cascade typical of 2D turbulent systems (Kraichnan & Montgomery 1980). Recent high-resolution direct numerical simulations have confirmed this theoretical value in both forced (Boffetta 2007) and decaying (Lindborg & Vallgren 2010; Fox & Davidson 2010) 2D turbulence. However, the slope in the inertial subrange differs from -3, but reaches the value of $-11/3$, as illustrated also in figure 5(*b*) by the power-law fit of the temporal spectra. This discrepancy is not surprising. To have a classical k^{-3} spectrum, we must have a significant range of fine-scale filaments, which is not the case in our simulations, where coherent vortices dominate the mixing layer evolution. According to Dritschel *et al.* (2008), such coherent vortices usually lead to steeper spectra. In particular, the value of $-11/3$ is not uncommon for the spectrum of 2D turbulent mixing layers. For example, it was also found by Lesieur *et al.* (1988). From a kinematic point of view, Gilbert (1988) has explained that such $k^{-11/3}$ is due to spiralling effects of the coherent vortices.

We next compute the turbulent kinetic energy $K(x, y) = K_{2D}(x, y) + K_{span}(x, y)$, where $K_{2D}(x, y) = 0.5[u^2_{rms}(x, y) + v^2_{rms}(x, y)]$, $K_{span}(x, y) = w^2_{rms}(x, y)$ and $u_{rms}(x, y) = \sqrt{|\overline{u^2}(x, y) - \bar{u}^2(x, y)|}$ (same notation for v_{rms} and w_{rms}). Figure 6 illustrates the behaviour of (*a*) the turbulent kinetic energy averaged in the y direction K_y, (*b*) its 2D part $K_{y,2D}$, (*c*) its spanwise part $K_{y,span}$ and (*d*) the percentage of spanwise energy with respect of the total energy. Two-dimensional turbulent mixing layers ($L_z = 0.125$

https://doi.org/10.1017/jfm.2014.85 Published online by Cambridge University Press

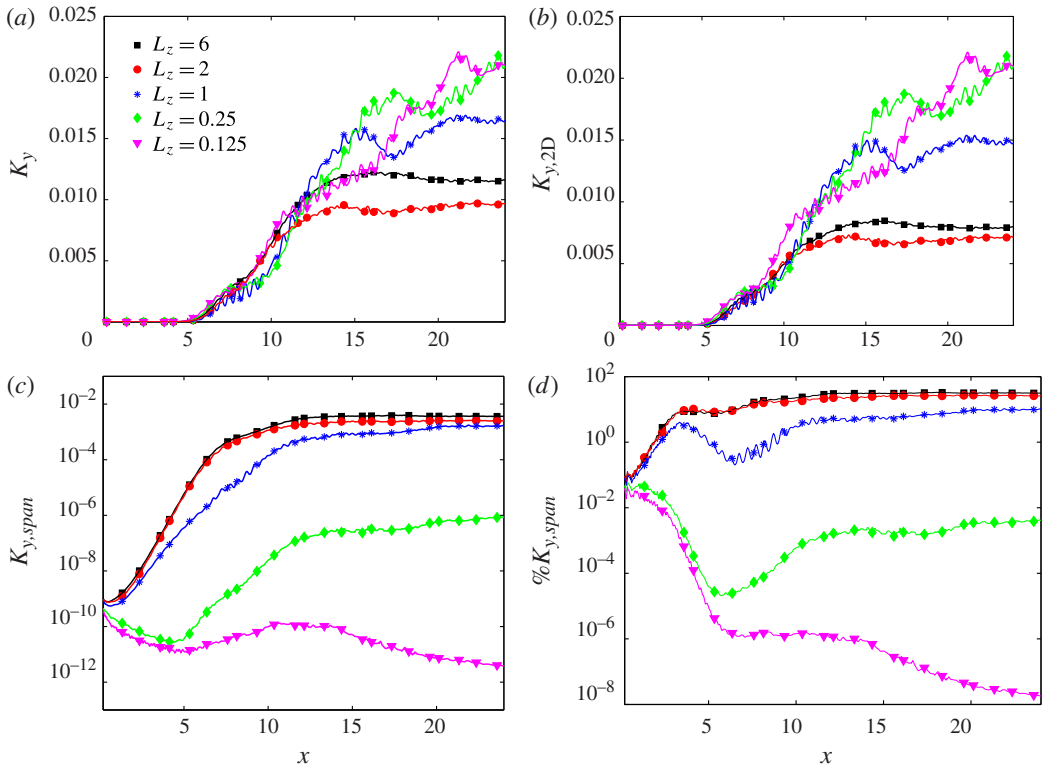


FIGURE 6. (Colour online) (*a*) The turbulent kinetic energy averaged along the y direction K_y, (*b*) its 2D part $K_{y,2D}$, (*c*) its spanwise part $K_{y,span}$ and (*d*) the percentage of spanwise energy into the total turbulent kinetic energy K_y versus the streamwise direction. The vertical axes of panels (*c*) and (*d*) are in log scale. The legend is the same as for figure 4(*a*).

and $L_z = 0.25$) have values of the turbulent kinetic energy that are larger than those characterized by fully 3D turbulence ($L_z = 2$ and $L_z = 6$), as illustrated in figure 6(*a*). Smith *et al.* (1996) have found a similar result in forced rotating turbulence. Moreover, the kinetic energy grows linearly along the x direction for the most confined domains. On the other hand, for $L_z = 2$ and $L_z = 6$, after an initial transient necessary to build up the turbulent cascade, the kinetic energy attains a statistically constant value. The case with $L_z = 1$ presents an evolution of the kinetic energy intermediate between those of 2D and 3D turbulent mixing layers. This is another sign of the halfway 2D–3D behaviour of the turbulence of this configuration.

Into the largest domain, the 2D and spanwise parts of the kinetic energy have a similar evolution (figure 6*b*,*c*), while they behave differently in the most constricted domain. Into the latter configurations, the 2D part grows linearly as seen for the total turbulent kinetic energy. In fact, the spanwise energy seems to attain a constant value after a transient and reaches much smaller values. Finally, we notice in figure 6(*d*) that the smallest domains have negligible percentages of spanwise energy, especially if compared to the largest ones. This definitely points out the almost complete two-dimensionalization by constricting the domain. Furthermore, the percentage always increases along the domain for $L_z = 2$ and $L_z = 6$, whereas it decreases for $L_z = 0.25$ and $L_z = 0.125$, in particular close to the inlet. For the latter configurations,

https://doi.org/10.1017/jfm.2014.85 Published online by Cambridge University Press

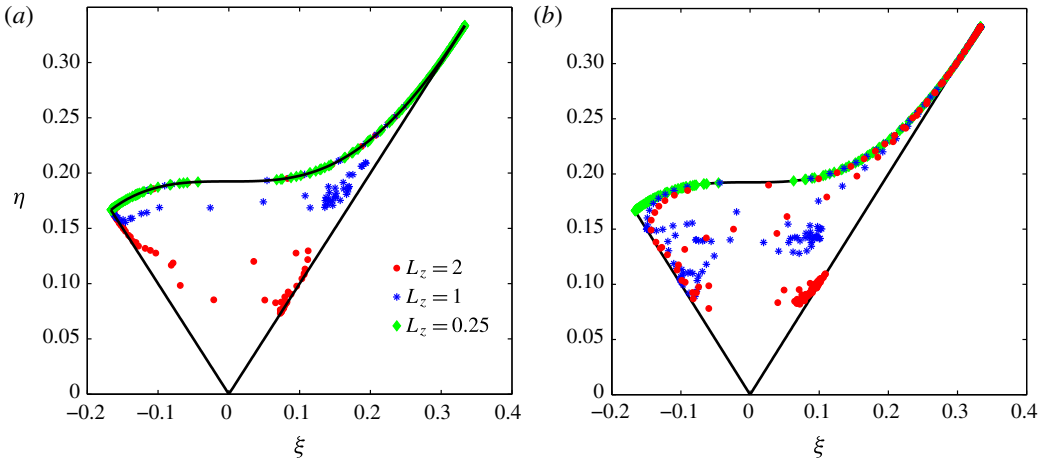


FIGURE 7. (Colour online) Sketch of the anisotropy tensor in the Lumley triangle constructed at (*a*) $x = 14$ and (*b*) $x = 22$.

the percentage of spanwise energy at the exit is smaller than at the entry. For $L_z = 1$, it increases, if a small region of the domain $3 < x < 7$ is excluded.

In order to study the anisotropy features of the systems, we show in figure 7 the so-called Lumley's triangle (Lumley 1978; Pope 2000) for $L_z = 0.25$ (diamonds), $L_z = 1$ (asterisks) and $L_z = 2$ (circles) at two different abscissas, (*a*) $x = 14$ and (*b*) $x = 22$. Such diagrams illustrate the behaviour of the non-null invariants, η and ξ, of the anisotropy tensor $\bar{\boldsymbol{b}}(x, y)$. The anisotropy tensor is defined as the deviatoric part of the Reynolds stress tensor normalized by its trace, i.e. by twice the turbulent kinetic energy. In fact, the state of anisotropy can be characterized by just these two invariants (ξ, η), defined as $6\xi^3 = \bar{b}_{ij}\bar{b}_{jk}\bar{b}_{ki}$ and $6\eta^2 = \bar{b}_{ij}\bar{b}_{jk}$. Every realizable Reynolds stress that can occur in a turbulent flow corresponds to a point inside the triangle depicted in figure 7. Each point corresponds to the invariants into a given y crossflow value.

First, we observe that the points associated with the non-null invariants of the anisotropy tensor remain within the region delimited by the three solid lines. This points out that our LES results follow the realizability diagram of Lumley (Lumley 1978; Pope 2000). For $L_z = 0.25$, the points are located on the upper side of the triangle. This means that the turbulence is characterized by fully 2D anisotropy (Pope 2000). By increasing the depth to $L_z = 1$, one can note the presence of points also inside the triangle, especially at $x = 22$. Finally, for $L_z = 2$, the location of the points is similar to the experiments on a 3D turbulent mixing layer conducted by Bell & Mehta (1990), as shown in Pope (2000). In particular, the Reynolds stresses at the centre of the mixing layer are close to being axisymmetric with ξ positive. On the other hand, the Reynolds stresses at the edges of the mixing layer are still close to axisymmetric but with ξ negative. Outside the shear layer, the anisotropy is (or is close to) two-component.

Finally, we illustrate in figure 8(*a*) the behaviour along the domain of the spanwise componenent of vortex stretching $VS_z = [\overline{\boldsymbol{\omega} \cdot \boldsymbol{\nabla} \boldsymbol{u}}]_z$ averaged along the y direction. The vortex stretching is null in an ideal fully 2D turbulent flow being typical of 3D flows. The vortex stretching may induce the formation of secondary quasi-streamwise vortices, which can break the primary structures, originating smaller vortical structures (Brancher, Chomaz & Huerre 1994). Analyses of the vortex stretching give a measure

https://doi.org/10.1017/jfm.2014.85 Published online by Cambridge University Press

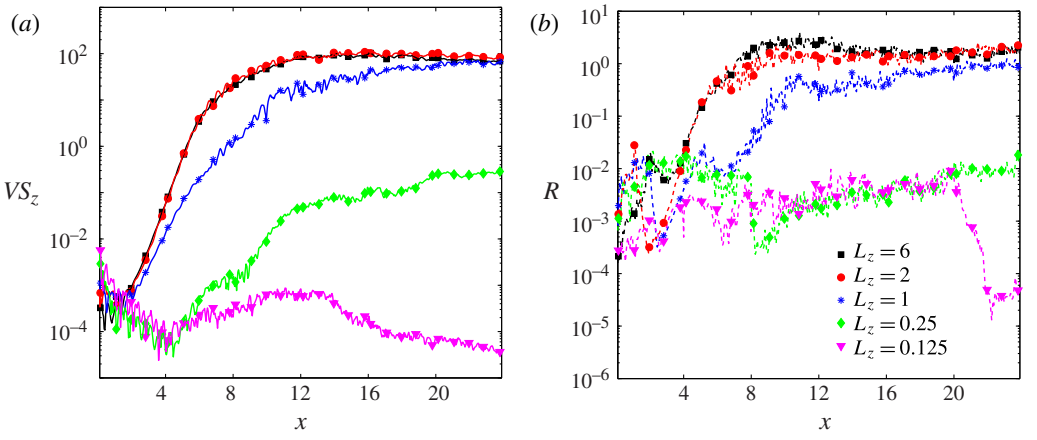


FIGURE 8. (Colour online) (*a*) The spanwise component of the vortex stretching VS_z averaged along the y direction and (*b*) the ratio R between $|\boldsymbol{VS}|$ and $|\boldsymbol{AT}|$ versus the streamwise direction. The legend is the same as figure 4(*a*).

of the strength of this process. The z components of the vortex stretching of 2D turbulent cases are much smaller with respect to those of 3D turbulent mixing layers. There is a difference of three (six) orders of magnitude between $L_z = 0.25$ ($L_z = 0.125$) and the least confined mixing layers. The same behaviour occurs for the other two components of the vortex stretching: VS_x and VS_y. However, the vortex stretching can be considered negligible if it is much weaker than the advection term $\boldsymbol{AT} = \overline{\boldsymbol{u} \cdot \boldsymbol{\nabla} \boldsymbol{\omega}}$. Thus, we illustrate in figure 8(*b*), the behaviour along the x direction of the ratio between the vortex stretching and the advection term $R = |\boldsymbol{VS}|/|\boldsymbol{AT}|$. The vortex stretching and the advection term are of the same order of magnitude for the configurations with $L_z \geqslant 1$. On the contrary, the maximum value of this ratio is around 10^{-2} for $L_z = 0.25$ and $L_z = 0.125$. We can conclude that for the smallest domain the vortex stretching is not strong enough to create secondary 3D instabilities while causing the two-dimensionalization.

3.3. *Discussion*

We have shown that the mixing layer spread and the turbulence isotropicity may be deeply altered by varying the domain depth. In particular, a two-dimensionalization can be obtained by confining the mixing layer along the spanwise direction.

A similar result was noticed by Biancofiore *et al.* (2012) in spatially developing turbulent wakes. They varied the height (L_y) of the domain to study the effect of the confinement along the crossflow direction with a constant depth (L_z). Then, it seems that the ratio between the height and the depth of the domain in spatial shear flows plays a role on the turbulent behaviour. This is also confirmed by the present work. However, in shear flows, such as wakes and mixing layers, the important length scale is not the height, but the momentum thickness (Ho & Huerre 1984). On the other hand, the growth of the local thickness in shear flows depends on the height (Biancofiore, Gallaire & Pasquetti 2011). Moreover, the spanwise wavelength of the 3D secondary instability in mixing layers is strictly related to the momentum thickness (Ho & Huerre 1984). The average spanwise spacing of the secondary structures increases with the mixing layer downstream evolution and remains of the

https://doi.org/10.1017/jfm.2014.85 Published online by Cambridge University Press

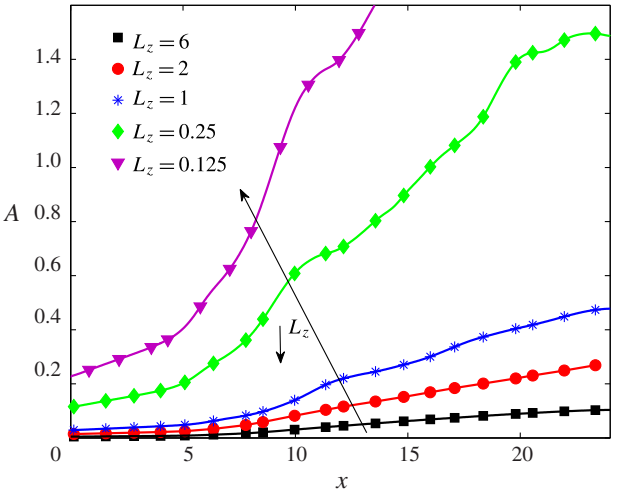


FIGURE 9. (Colour online) The behaviour of the aspect ratio $A = \theta/(L_z/2)$ along the streamwise direction x. The aspect ratio is a rescaling of the momentum thickness (figure 4*a*) with the confining scale. The legend is the same as figure 4(*a*).

same order of magnitude as the local thickness. Thus, we suggest that the aspect ratio that plays a role to define the turbulence nature is the ratio between the momentum thickness and the confining transverse scale. Since the spanwise direction is periodic, the maximum transverse reference scale is the half-depth $L_z/2$.

Hence, we depict in figure 9 the behaviour of the aspect ratio $A = \theta/(L_z/2)$ along the streamwise direction. The aspect ratio is larger for the smallest domains, $L_z = 0.25$ and $L_z = 0.125$, depicted by diamonds and triangles, respectively. In particular, for such configurations, the momentum thickness reaches the value of the confining scale, i.e. the aspect ratio reaches the value $A = 1$. Note that these two configurations are characterized by an almost fully 2D turbulence. When 3D structures are present in the mixing layer, the aspect ratio is far from unity.

In conclusion, we can define a criterion to discriminate between 2D and 3D turbulent mixing layers, as given in Rayleigh–Taylor convection by Boffetta *et al.* (2012). When the scale of the turbulent structures reaches the confining scale (i.e. the half-depth $L_z/2$), we have a strong two-dimensionalization of the turbulence. This could be explained by relating the momentum thickness to the spanwise wavelength of the secondary instability. Since they are of the same of order of magnitude, we can imagine that an aspect ratio larger than unity means that the secondary instability does not have enough space to develop. Then the flow becomes or remains 2D. The behaviour of the vortex stretching (see figure 8) seems to confirm this hypothesis.

4. Conclusions

For the first time, we have analysed the influence of a geometric constraint on the turbulent nature of spatially developing shear flows, in particular, a mixing layer, by means of LES. The study focused on the crossover between 2D and 3D turbulence in such flows. Several quantities, such as temporal Fourier spectra, Lumley's diagrams, turbulent kinetic energy and vortex stretching, have been presented. We have found a two-dimensionalization due to geometric anisotropy, as already noticed in several

https://doi.org/10.1017/jfm.2014.85 Published online by Cambridge University Press

physical systems, such as forced turbulent systems (Smith *et al.* 1996; Celani *et al.* 2010), electromagnetically driven flows (Shats *et al.* 2010; Xia *et al.* 2011) and, more recently, thermal convection (Boffetta *et al.* 2012). The crossover occurs for a depth in the range $0.25 < L_z < 2$. This is also confirmed by the intermediate 2D–3D turbulent character shown by the mixing layer with $L_z = 1$.

Furthermore, the constraint along the spanwise direction causes a deceleration in the growth of the mixing layer. A consequence of such deceleration is the larger aspect ratio $A = \theta/(L_z/2)$ reached by a 2D turbulent mixing layer. We conclude that when the turbulent structures are of the same order of magnitude as the confining scale, the mixing layer has almost a fully 2D behaviour. In particular, secondary structures due to the deformation of the primary rolls are strongly hindered by decreasing the depth of the domain, as illustrated by the behaviour of the vortex stretching.

The present work opens interesting perspectives on two-dimensionalization due to geometric anisotropy. A similar study could be conducted on other spatial developing shear flows, such as jets or wakes. Furthermore, in confined flows, the presence of boundary layers influences the turbulent behaviour. Therefore, the effect of boundary layers on the crossover between 2D and 3D turbulence due to geometric anisotropy is another important aspect to study. This kind of analysis can be conducted both numerically and experimentally.

Acknowledgements

The calculations have been carried out on the computer of Mesocentre SIGAMM of the OCA (Observatoire de la Côte Azur). S. Musacchio, E. Lindborg, F. Picano and R. Pasquetti are warmly acknowledged for stimulating discussions.

REFERENCES

BELL, J. H. & MEHTA, R. D. 1990 Development of a two-stream mixing layer from tripped and untripped boundary layers. *AIAA J.* **28**, 2034–2042.

BERNAL, L. P. & ROSHKO, A. 1986 Streamwise vortex structure in plane mixing layers. *J. Fluid Mech.* **170**, 499–525.

BIANCOFIORE, L., GALLAIRE, F. & PASQUETTI, R. 2011 Influence of confinement on a two-dimensional wake. *J. Fluid Mech.* **688**, 297–320.

BIANCOFIORE, L., GALLAIRE, F. & PASQUETTI, R. 2012 Influence of confinement on obstacle-free turbulent wakes. *Comput. Fluids* **58**, 27–44.

BOFFETTA, G. 2007 Energy and enstrophy fluxes in the double cascade of two-dimensional turbulence. *J. Fluid Mech.* **589**, 253–260.

BOFFETTA, G., DE LILLO, F., MAZZINO, A. & MUSACCHIO, S. 2012 Bolgiano scale in confined Rayleigh–Taylor turbulence. *J. Fluid Mech.* **690**, 426–440.

BOFFETTA, G. & ECKE, R. E. 2012 Two-dimensional turbulence. *Annu. Rev Fluid Mech.* **44**, 427–451.

BOFFETTA, G. & MUSACCHIO, S. 2010 Evidence for the double cascade scenario in two-dimensional turbulence. *Phys. Rev.* E **82**, 016307.

BRANCHER, P., CHOMAZ, J.-M. & HUERRE, P. 1994 Direct numerical simulations of round jets: vortex induction and side jets. *Phys. Fluids* **6**, 1768–1774.

BROWN, G. L. & ROSHKO, A. 1974 On density effects and large structures in turbulent mixing layers. *J. Fluid Mech.* **64**, 775–816.

CELANI, A., MUSACCHIO, S. & VINCENZI, D. 2010 Turbulence in more than two and less than three dimensions. *Phys. Rev. Lett.* **104**, 184506.

CHANDRSUDA, C., MEHTA, R. D., WEIR, A. D. & BRADSHAW, P. 1978 Effect of free-stream turbulence on large structure in turbulent mixing layers. *J. Fluid Mech.* **85**, 693–704.

https://doi.org/10.1017/jfm.2014.85 Published online by Cambridge University Press

CHOLET, J.-P. & LESIEUR, M. 1981 Parametrization of small scales of three dimensional isotropic turbulence utilizing spectral closures. *J. Atmos. Sci.* **38**, 2747–2757.

COMTE, P., LESIEUR, M. & LAMBALLAIS, E. 1992 Small scale stirring of vorticity and a passive scalar in a 3D temporal mixing layer. *Phys. Fluids* A **4**, 2761–2778.

COMTE, P., SILVESTRINI, J. H. & BÉGOU, P. 1998 Streamwise vortices in large-eddy simulations of mixing layers. *Eur. J. Mech.* B **17**, 615–637.

DRITSCHEL, D. G., SCOTT, R. K., MACASKILL, C., GOTTWALD, G. A. & TRAN, C. V. 2008 Unifying scaling theory for vortex dynamics in two-dimensional turbulence. *Phys. Rev. Lett.* **101**, 094501.

FOX, S. & DAVIDSON, P. A. 2010 Freely decaying two-dimensional turbulence. *J. Fluid Mech.* **659**, 351–364.

GILBERT, A. D. 1988 Spiral structures and spectra in two-dimensional turbulence. *J. Fluid Mech.* **193**, 475–497.

HO, C.-M. & HUERRE, P. 1984 Perturbed free shear layer. *Annu. Rev. Fluid Mech.* **16**, 365–424.

KARAMANOS, G. S. & KARNIADAKIS, G. E. 2000 A spectral vanishing viscosity method for large-eddy simulation. *J. Comput. Phys.* **163**, 22–50.

KRAICHNAN, R. H. & MONTGOMERY, D. 1980 Two-dimensional turbulence. *Rep. Prog. Phys.* **43**, 547–619.

LESIEUR, M., STAQUET, C., LE ROY, P. & COMTE, P. 1988 The mixing layer and its coherence examined from the point of view of two-dimensional turbulence. *J. Fluid Mech.* **192**, 511–534.

LINDBORG, E. & VALLGREN, A. 2010 Testing Batchelor's similarity hypotheses for decaying two-dimensional turbulence. *Phys. Fluids* **22**, 091704.

LUMLEY, J. L. 1978 Computational modeling of turbulent flows. *Adv. Appl. Mech.* **18**, 123–176.

MADAY, Y., OULD KABER, S. M. & TADMOR, E. 1993 Legendre pseudo-spectral viscosity method for nonlinear conservation laws. *SIAM J. Numer. Anal.* **30** (2), 321–342.

MINGUEZ, M., PASQUETTI, R. & SERRE, E. 2008 High-order large-eddy simulation of flow over a simplified car model. *Phys. Fluids* **20**, 095101.

NGAN, K., STRAUB, D. & BARTELLO, P. 2005 Aspect ratio effects in quasi-two-dimensional turbulence. *Phys. Fluids* **17**, 125102.

NGAN, K., STRAUB, D. & BARTELLO, P. 2008 Dissipation of synoptic-scale flow by small-scale turbulence. *J. Atmos. Sci.* **65**, 766–791.

PASQUETTI, R. 2005 Spectral vanishing viscosity method for LES: sensitivity to the SVV control parameters. *J. Turbul.* **6**, N12.

PASQUETTI, R. 2006 Spectral vanishing viscosity method for large-eddy simulation of turbulent flows. *J. Sci. Comput.* **27**, 365–375.

PASQUETTI, R. 2010 Temporal/spatial simulation of the stratified far wake of a sphere. *Comput. Fluids* **40**, 179–187.

PICANO, F. & HANJALIĆ, K. Leray-α regularization of the Smagorinsky-closed filtered equations for turbulent jets at high Reynolds numbers. *Flow Turbul. Combust.* **89** (4), 627–650.

PIERREHUMBERT, R. T. & WIDNALL, S. E. 1982 The two- and three-dimensional instabilities of a spatially periodic shear layer. *J. Fluid Mech.* **114**, 59–82.

POPE, S. B. 2000 *Turbulent Flows*. Cambridge University Press.

SABBAH, C. & PASQUETTI, R. 1998 A divergence-free multi-domain spectral solver of the Navier–Stokes equations in geometries of high aspect ratio. *J. Comput. Phys.* **139**, 359–379.

SHATS, M., BYRNE, D. & XIA, H. 2010 Turbulence decay rate as a measure of flow dimensionality. *Phys. Rev. Lett.* **105**, 264501.

SMITH, L. M., CHASNOV, J. R. & WALEFFE, F. 1996 Crossover from two- to three-dimensional turbulence. *Phys. Rev. Lett.* **77**, 2467–2470.

WINANT, C. D. & BROWAND, F. K. 1974 Vortex-pairing, the mechanism of turbulent mixing layer growth at moderate Reynolds number. *J. Fluid Mech.* **63**, 237–255.

XIA, J., BYRNE, D., FALKOVICH, D. & SHATS, M. 2011 Upscale energy transfer in thick turbulent fluid layers. *Nat. Phys.* **7**, 321–324.

XU, C. J. & PASQUETTI, R. 2004 Stabilized spectral element computations of high Reynolds number incompressible flows. *J. Comput. Phys.* **196**, 680–704.

https://doi.org/10.1017/jfm.2014.85 Published online by Cambridge University Press